Phosphonic Acid-Functionalized Diblock Copolymer Nano-Objects via Polymerization-Induced Self-Assembly: Synthesis, Characterization and Occlusion into Calcite Crystals

Andreas Hanisch,[a] Pengcheng Yang,[a] Alexander N. Kulak,[b] Lee A. Fielding,[a] Fiona C. Meldrum[b] and Steven P. Armes[*,a]*

[a] Dainton Building, Department of Chemistry, The University of Sheffield, Brook Hill, Sheffield, South Yorkshire, S3 7HF, UK.

[b] School of Chemistry, University of Leeds, Woodhouse Lane, Leeds, LS2 9JT, UK.

Abstract. Dialkylphosphonate-functionalized and phosphonic acid-functionalized macromolecular chain transfer agents (macro-CTAs) were utilized for the reversible addition–fragmentation chain transfer (RAFT) dispersion polymerization of benzyl methacrylate (BzMA) at 20% w/w solids in methanol at 64 °C. Spherical, worm-like and vesicular nano-objects could all be generated through systematic variation of the mean degree of polymerization of the core-forming PBzMA block when using relatively short macro-CTAs. Construction of detailed phase diagrams is essential for the reproducible targeting of pure copolymer morphologies, where these were characterized using transmission electron microscopy (TEM) and dynamic light scattering (DLS). For nano-objects prepared using the phosphonic acid-based macro-CTA, transfer from methanol dispersion to water leads to the development of anionic surface charge as a result of ionization of the stabilizer chains, but this does not adversely affect the copolymer morphology. Given the well-known strong affinity of phosphonic acid for calcium ions, selected nano-objects were evaluated for their *in-situ* occlusion within growing $CaCO_3$ crystals. Scanning electron microscopy (SEM) studies provide convincing evidence for the occlusion of both worm-like and vesicular phosphonic acid-based nano-objects and hence the production of a series of interesting new organic-inorganic nanocomposites.

* Author to whom correspondence should be addressed (s.p.armes@sheffield.ac.uk)

INTRODUCTION

It is well-known that phosphorus-based polymers have a wide range of potential applications. They bind to metal ions,[1,2] adsorb strongly onto metal oxide surfaces[3] and biominerals,[4,5] can serve as proton exchange membrane material,[6] allow the design of halogen-free flame-retardant materials,[7-9] and can exhibit excellent biocompatibility.[10,11] Literature examples include organophosphorus polymers based on *e.g.* methacrylate-type[12,13] or acrylamide-type[14] dialkylphosphonates. Anionic polyelectrolytes are also accessible either directly by polymerization of the free acid phosphate,[15] phosphonate[6,13] or phosphinate[16] monomers, or via hydrolysis of dialkylphosphonate polymers.[13,14] DNA is a particularly important example of a naturally-occurring anionic polyphosphate.[17] Furthermore, phosphorus-based polymers can also exhibit cationic (*e.g.* phosphonium-based polymers[18]) or zwitterionic character (*e.g.* poly(2-(methacryloyloxy)ethyl phosphorylcholine), or PMPC).[19,20] Both materials are of considerable interest in the field of biomaterials.[21,22]

Recent progress in the development of controlled/living polymerization methods such as atom transfer radical polymerization (ATRP)[23] and reversible addition-fragmentation transfer (RAFT) polymerization[24] has facilitated the design of a wide range of well-defined controlled-structure polymers. Many examples of well-defined PMPC-based diblock copolymers have been prepared by ATRP[25,26] and RAFT.[27,28] Of particular relevance to the present study, (1-ethoxycarbonyl)vinyl dimethylphosphate was homopolymerized *via* ATRP and also copolymerized using either polystyrene or poly(methyl methacrylate) macro-initiators.[29] While control over the polymerization of this dialkylphosphate monomer was rather poor – such that incomplete conversions or broad molecular weight distributions ($M_w/M_n > 1.60$) were obtained depending on the choice of catalyst – subsequent hydrolysis produced the corresponding phosphoric acid-based

diblock copolymers. In contrast, RAFT polymerization of either 2-(acryloyloxy)ethyl phosphate or 2-(methacryloyloxy)ethyl phosphate yielded well-defined diblock copolymers when employing 2-(acetoacetoxy) ethyl methacrylate as the second block.[30] Divinyl impurities present in both phosphate monomers limited the molecular weight of the first block to 20 000 g mol^{-1}, but otherwise, extensive crosslinking was observed.

As far as we are aware, vinylphosphonic acid (VPA) was the first example of a monomer bearing an unprotected phosphonic acid to be polymerized directly *via* RAFT polymerization.[31] As yet, however, only diblock copolymers with relatively low molecular weights were obtained with this approach. Considerably higher molecular weights have been reported for the ATRP of 4-vinylbenzyl diethylphosphonate and relatively narrow molecular weight distributions were achieved in this case.[6] Both deprotection (to generate the free phosphonic acid groups) and chain extension (from a polystyrene macro-initiator) were demonstrated for this styrenic monomer.[32] Similarly, well-defined homopolymers and diblock copolymers were obtained when using 2-(acrylamido)ethyl diethylphosphonate, with subsequent hydrolysis producing the corresponding free phosphonic acid-based polymers.[14]

Another phosphorus-based monomer, methacryloyloxymethyl dimethylphosphonate (MP) has recently become commercially available, but attempts to polymerize this monomer *via* ATRP have only resulted in rather low conversions and relatively low molecular weights, presumably due to strong copper complexation.[33] In this context, RAFT polymerization offers a potentially decisive advantage, since it involves an organosulfur-based chain transfer agent rather than a transition metal catalyst. Moreover, phosphonic acid-based homopolymers were recently prepared directly *via* RAFT polymerization.[13] In principle, a wide range of functional diblock copolymers

incorporating either dialkylphosphonate or phosphonic acid repeat units should be accessible using this approach.

Recently, RAFT polymerization has also been exploited in the context of polymerization-induced self-assembly (PISA), which is a highly efficient and versatile method for directly generating diblock copolymer nano-object dispersions at relatively high solids (up to 50% w/w).[34-37] In such formulations, a soluble macromolecular chain transfer agent is extended with a monomer to form a new block, which becomes increasingly insoluble in the reaction medium. The first soluble block confers steric stabilization, while the growing insoluble block drives *in situ* self-assembly. Varying the relative block volume fractions while conducting such syntheses at various copolymer concentrations allows predictive phase diagrams to be constructed, which are essential for the reproducible generation of pure phases comprising spherical, worm-like or vesicular diblock copolymer nanoparticles.[38] This PISA approach has been shown to be generic. Various formulations have been reported in aqueous solution,[39-46] lower alcohols,[47-55] *n*-alkanes,[56-58] toluene[59] and solvent mixtures[60,61] that provide access not only to non-ionic (or zwitterionic) nanoparticles,[42,62-65] but also anionic[66,67] or cationic nano-objects.[68] All of these aforementioned PISA formulations are based on dispersion polymerization, whereby the core-forming monomer is soluble in the reaction medium. There are also numerous examples of heterogeneous formulations based on aqueous emulsion polymerization.[69-76]

There are very few literature examples of PISA syntheses involving phosphorus-based monomers. In 2011 our group reported aqueous formulations based on a zwitterionic PMPC macromolecular chain transfer agent (macro-CTA) for the preparation of diblock copolymer nano-objects.[42,65] Very recently, Zhang *et al.* employed 4-diphenylphosphinostyrene as the core-forming monomer to prepare catalytically-active micellar nanoreactors.[77] However, we are not

aware of any examples involving anionic phosphate-based monomers. As mentioned earlier, Monge and co-workers recently reported the RAFT *solution* polymerization of methacryloyloxymethyl dimethylphosphonate (MP) and methacryloyloxymethyl phosphonic acid (MPA),[13] which are of potential interest for biomedical applications. In the present work, we describe the PISA synthesis of dialkylphosphonate- and phosphonic acid-functionalized diblock copolymer nano-objects using these two monomeric units. A range of nano-objects are prepared using a RAFT alcoholic dispersion polymerization formulation and characterized in terms of their size, morphology and surface chemistry. Occlusion of selected worm-like and vesicular nanoparticles within growing $CaCO_3$ crystals is also briefly studied as a potential route to novel organic-inorganic nanocomposites.

EXPERIMENTAL SECTION

Materials. Methacryloyloxymethyl dimethylphosphonate (MP; Specific Polymers, France), glycerol monomethacrylate (GMA; kindly donated by GEO Specialty Chemicals, Hythe, UK), 2-hydroxypropyl methacrylate (HPMA, Alfa Aesar, 98%), 2,2′-azobis(isobutyronitrile) (AIBN; Molekula, Germany), 4,4′-azobis(4-cyanopentanoic acid) (ACVA; Sigma-Aldrich, ≥ 98%), 1,3,5-trioxane (Sigma-Aldrich, UK), bromotrimethylsilane (TMSBr; Acros, 98%), $CaCl_2{\cdot}2H_2O$ (Sigma-Aldrich), and $(NH_4)_2CO_3$ (Sigma-Aldrich) were used as received. Benzyl methacrylate (BzMA, 96 % purity, Sigma-Aldrich) was passed through a column to remove inhibitor prior to its polymerization. 2-Cyano-2-propyl dithiobenzoate (CPDB; Strem Chemicals, UK) had a CTA efficiency of approximately 80%. This efficiency was taken into account for the RAFT syntheses of the various macro-CTAs. Methanol, ethanol and DMF were all of solvent-grade, while

anhydrous dichloromethane (DCM) was used for the hydrolysis experiments. Deuterated NMR solvents (CD_3OD and d_6-DMSO) were purchased from Cambridge Isotopes Laboratories, Inc.

Synthesis of Poly(methacryloyloxymethyl dimethylphosphonate) [PMP] Macro-CTA. The RAFT polymerization of MP was conducted as reported by Canniccioni *et al.*[13] using a 25% w/w MP solution in DMF and a CPDB/AIBN molar ratio of 3.0. In a typical protocol, the monomer (22.50 g, 108.1 mmol), CPDB (1.813 g, 4.9 mmol), and AIBN (266.3 mg, 1.6 mmol) were dissolved in 73 mL DMF in a 250 mL round-bottomed flask. After purging with nitrogen for 20 min, the flask was sealed and placed in a preheated oil bath at 70 °C for 3.5 h, before quenching the reaction by cooling with an ice-bath. Samples were taken during the course of polymerization for ^{1}H NMR measurements and the final conversion was determined to be 65%. The crude PMP was purified *via* precipitation into excess cold diethyl ether (twice) and finally freeze-dried from aqueous solution overnight. A mean degree of polymerization of 24 (or M_n= 5.2 kg mol^{-1}) was calculated *via* end-group analysis using ^{1}H NMR spectroscopy by comparing the integrated intensity of the two aromatic protons of the CTA at 7.42 – 7.56 ppm with the five protons assigned to the methacrylic backbone at 0.2 – 2.4 ppm. DMF GPC analysis indicated apparent M_n and M_w/M_n values of 5.4 kg mol^{-1} and 1.20, respectively. Two other PMP macro-CTAs were also prepared with higher target mean degrees of polymerization: DMF GPC indicated a M_n of 7.0 kg mol^{-1} and M_w/M_n = 1.23 for PMP_{32} and a M_n of 9.5 kg mol^{-1} and M_w/M_n = 1.22 for PMP_{42}.

Hydrolysis of Poly(methacryloyloxymethyl dimethylphosphonate) [PMP] yielding Poly(methacryloxymethylphosphonic acid) [PMPA]. To generate the free phosphonic acid form, PMP was hydrolyzed with trimethylsilyl bromide (TMSBr).[13] In a typical reaction, PMP_{24} (10.0 g) was dissolved in anhydrous DCM (100 mL), followed by addition of TMSBr (4 equiv. per phosphonate group). The reaction mixture was stirred for 3 h at 20 °C and then the solvent was

removed under reduced pressure. The free phosphonic acid homopolymer, PMPA, was generated by addition of methanol (500 mL) followed by stirring for 1 h at 20 °C. After concentration under reduced pressure, the crude polymer was purified *via* dialysis against water, followed by freeze-drying overnight. Aqueous GPC analysis of the three PMPA homopolymers using 30% methanol co-solvent at pH 9 gave the following data: $PMPA_{24}$ M_n = 10.1 kg mol^{-1}, M_w/M_n = 1.03; $PMPA_{32}$ M_n = 11.1 kg mol^{-1}, M_w/M_n = 1.03; $PMPA_{42}$ M_n = 12.6 kg mol^{-1}, M_w/M_n = 1.05.

Chain Extension Experiments with PMPA Macro-CTAs. Macro-CTAs were chain-extended with glycerol monomethacrylate (GMA) to examine their blocking efficiencies. RAFT solution polymerizations were conducted at 20% w/w solids at 64 °C for 16 h. In a typical protocol, the $PMPA_{24}$ macro-CTA (140.5 mg, 31.22 μmol), AIBN (1.0 mg, 6.24 μmol, CTA/AIBN molar ratio = 5.0), GMA (1.00 g, 6.24 mmol), and 1,3,5-trioxane (11.3 mg, 124.87 μmol, GMA/1,3,5-trioxane molar ratio = 50) were dissolved in methanol (4.0 mL). The solution was purged with nitrogen for 20 min and then the sealed vial was placed in a preheated oil bath at 64 °C for 16 h, before quenching the reaction by cooling with an ice-bath. Samples were taken during the course of the polymerization for ^{1}H NMR measurements. For three different blocking experiments, final GMA monomer conversions were determined to lie between 46 and 73%. The resulting PMPA-PGMA diblock copolymers were precipitated twice from cold diethyl ether and freeze-dried from aqueous solution overnight prior to analysis by aqueous GPC (with 30% methanol co-solvent at pH 9): $PMPA_{24}$-$PGMA_{140}$ M_n= 18.3 kg mol^{-1}, M_w/M_n = 1.05; $PMPA_{32}$-$PGMA_{146}$ M_n = 20.0 kg mol^{-1}, M_w/M_n = 1.07; $PMPA_{42}$-$PGMA_{92}$ M_n = 19.5 kg mol^{-1}, M_w/M_n = 1.07.

Diblock Copolymer Synthesis *via* Alcoholic Dispersion Polymerization. Alcoholic RAFT dispersion polymerizations were conducted with both the dialkylphosphonate (PMP) macro-CTAs as well as the phosphonic acid (PMPA) macro-CTAs at 20% w/w solids under identical conditions.

In a typical synthesis targeting a diblock composition of $PMPA_{24}$-$PBzMA_{300}$, the protocol was as follows: PMPA macro-CTA (37.5 mg, 8.32 μmol), AIBN (0.30 mg, 1.67 μmol, CTA/AIBN molar ratio = 5.0), and BzMA (440 mg, 2.50 mmol) were weighed into a sample vial and dissolved in pre-degassed methanol (1.91 g). This vial was then sealed with a septum and purged using a gentle nitrogen flow for 10 min while cooling in ice to minimize evaporation. Polymerization was initiated by placing the vial in a preheated oil bath at 64 °C. In order to guarantee a high BzMA conversion, the polymerization was conducted at this temperature for 24 h before quenching by exposure to air. In the case of the alcoholic dispersion polymerization syntheses conducted using the PMP macro-CTAs, the final PMP-PBzMA diblock copolymers were also analyzed using DMF GPC (see Table 1 and Table 3 for details).

$CaCO_3$ Precipitation *via* the Ammonia Diffusion Method.[78] For the crystallization experiments, 50 μL of a 1.0% w/w aqueous copolymer dispersion were diluted with water (2.50 mL) and a 3 mM $CaCl_2$ solution (2.50 mL) in a 30 mL sample vial, giving a final 0.01% w/w copolymer dispersion in a 1.5 mM $CaCl_2$ aqueous solution. A glass slide which had been pre-cleaned with piranha solution was placed on the base of the vial and then the samples were transferred to a desiccator previously charged with $(NH_4)_2CO_3$ powder (5.0 g). Crystallization was allowed to proceed for 24 h at 20 $^{\circ}$C, then the glass slides were removed from solution, washed with deionized water and ethanol, and finally air-dried. A second set of crystallization experiments was also conducted using a 0.005% w/w aqueous copolymer dispersion. Controll experiments were conducted in the absence of added copolymer.

Characterization. NMR Spectroscopy. ^{1}H NMR spectra were recorded in d_6-DMSO for PMP and PMPA and their related diblock copolymers using either a 400 MHz or 250 MHz Bruker spectrometer. A spectrum of the PGMA homopolymer was also recorded in CD_3OD. ^{31}P NMR

spectra for the PMP and PMPA macro-CTAs were recorded in d_6-DMSO using a 250 MHz Bruker spectrometer (400 scans).

Gel Permeation Chromatography (GPC). GPC analyses of PMP and PGMA homopolymers and PMP-PBzMA diblock copolymers were conducted using two Polymer Laboratories PL gel 5 μm mixed C columns and one PL polar gel 5 μm guard column arranged in series and maintained at 60°C, followed by a Varian 390 LC refractive index detector. The DMF eluent contained 10 mM LiBr, and the flow rate was 1.0 mL min^{-1}. Calibration was achieved using a series of near-mondisperse poly(methyl methacrylate) standards (ranging from 645 g mol^{-1} up to 2.48 x 10^6 g mol^{-1}). Molecular weight distributions for the PMPA and PMPA-PGMA diblock copolymers were assessed using aqueous GPC, which comprised an Agilent 1260 Infinity set-up fitted with two Agilent PS Aquagel-OH 8 µm columns at 35 °C and a refractive index detector. The eluent was a 10 mM NaH_2PO_4 pH 9 buffer containing 200 mM $NaNO_3$ and 30% methanol at a flow rate of 1.0 ml min^{-1}. Calibration was achieved using a series of near-monodisperse poly(methacrylic acid) standards ranging from 1.27 to 4.83 x 10^5 g mol^{-1}.

Dynamic Light Scattering (DLS) and Zeta Potential Measurements. Intensity-average hydrodynamic diameters of the dispersions were obtained by DLS using a Malvern Zetasizer NanoZS instrument. This instrument detects scattered light at an angle of 173° and was equipped with a 4 mW He-Ne laser operating at 633 nm, an avalanche photodiode detector with high quantum efficiency, and an ALV/LSE-5003 multiple τ digital correlator electronics system. Copolymer dispersions of ~ 0.20% w/w solids were analyzed using the cumulants method to obtain the hydrodynamic (z-average) diameter and polydispersity index (PDI). Aqueous electrophoresis studies were performed on 0.01% w/w copolymer dispersions using the same instrument equipped

with DTS1070 cells. The solution pH was adjusted by the manual addition of 0.01-1.0 M HCl or NaOH, and the background electrolyte was 1 mM NaCl.

Transmission Electron Microscopy (TEM). Copolymer particle morphologies were assessed using a Philips CM 100 instrument operating at 100 kV and equipped with a Gatan 1k CCD camera. For sample preparation, 8 μL of a diluted copolymer dispersion (~ 0.20% w/w) was dropped onto a freshly glow-discharged grid, left for 30 s, and then blotted with filter paper to remove excess solution. Subsequently, staining was performed for 30 s using a 8 μL droplet of 0.75% w/v uranyl formate solution, followed by blotting the excess stain and drying with a vacuum hose. TEM grids were prepared by coating copper/palladium TEM grids (Agar Scientific, UK) with a thin film of amorphous carbon.

Optical Microscopy, Scanning Electron Microscopy (SEM) and Raman Microscopy. The dimensions and morphologies of the $CaCO_3$ (calcite) crystals were assessed using optical microscopy and scanning electron microscopy. Optical microscopy images of crystals grown on glass slides were recorded using a Motic DMBA 300 digital biological microscope with a built-in camera and analyzed using Motic Images 2.0 ML software. For SEM studies, the glass slides supporting the $CaCO_3$ crystals were mounted on SEM stubs using adhesive pads. Imaging of the uncoated samples was performed using a FEI Nova NanoSEM 450 operating at 2 kV. Cross-sections of the $CaCO_3$ crystals were also imaged using SEM to investigate the extent of particle occlusion. Such samples were prepared by placing a clean glass slide on top of the glass slide coated with $CaCO_3$ crystals and pressing down while slightly twisting the upper glass slide. This protocol resulted in fracture of the crystals, hence revealing their interior structure. Characterization of the crystal polymorph was conducted via Raman microscopy studies of

individual particles using a Renishaw Raman 200 System microscope operating at a laser wavelength of 785 nm.

RESULTS AND DISCUSSION

Synthesis of Poly(methacryloyloxymethyl dimethylphosphonate) and Poly(methacryloyloxymethyl phosphonic acid) Macro-CTAs.

Methacryloyloxymethyl dimethylphosphonate (MP) was used for the synthesis of the macro-CTA in order to prepare phosphonic acid-stabilized nano-objects *via* RAFT dispersion polymerization. The RAFT solution polymerization of this commercially available monomer was recently studied using 2-cyano-2-propyl dithiobenzoate as chain transfer agent.[13] The resulting PMP macro-CTA can subsequently be converted into PMPA *via* ester hydrolysis, see Scheme 1. Three near-monodisperse PMP macro-CTAs with DPs of 24, 32 or 42 were synthesized in DMF at 70 °C. The corresponding DMF GPC traces are shown in Figure 1a; M_w/M_n values were below 1.25 in each case. Subsequent hydrolysis in dichloromethane with trimethylsilyl bromide and methanol yields the corresponding PMPA in its free phosphonic acid form, as indicated by a shift from 21.6 ppm to 14.0 ppm in the ^{31}P spectrum (Figure 1b and Figure S1). Because of unfavorable column interactions during attempted DMF GPC analysis, the PMPA macro CTAs had to be characterized using aqueous GPC (see Figure S2). These analyses indicated relatively low M_w/M_n values (less than 1.05).

Polymerization Induced Self-Assembly (PISA) in Aqueous and Alcoholic Media. First, the performance of the PMP macro-CTA as non-ionic stabilizer block for the aqueous dispersion polymerization of HPMA was investigated at pH 5. This facilitates comparison with later experiments conducted with the anionic PMPA macro-CTA, which is singly ionized at this pH.[13]

Scheme 1. RAFT Solution Polymerization of Methacryloyloxymethyl Dimethylphosphonate (MP) and Subsequent Hydrolysis of the PMP Precursor to Obtain Poly(methacryloyloxymethylphosphonic acid) (PMPA); RAFT Dispersion Polymerization of BzMA in Methanol Using Either the PMP or PMPA Macro-CTA as Steric Stabilizer Produced Spherical, Worm-like or Vesicular Nano-Objects, Depending on the Precise PISA Formulation

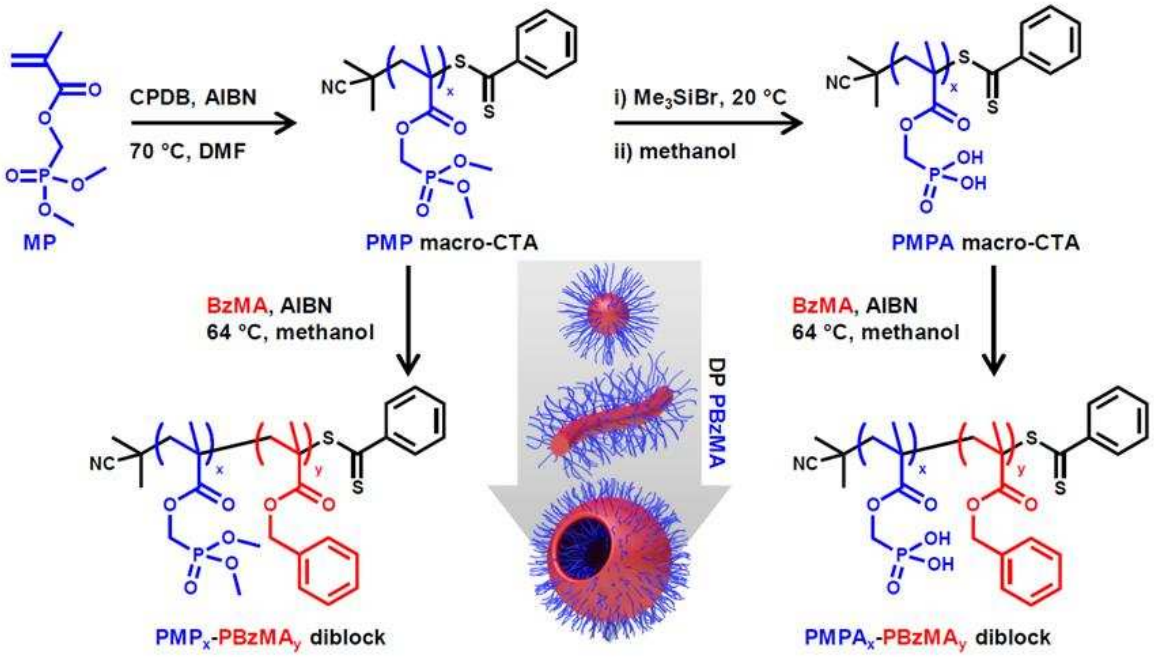

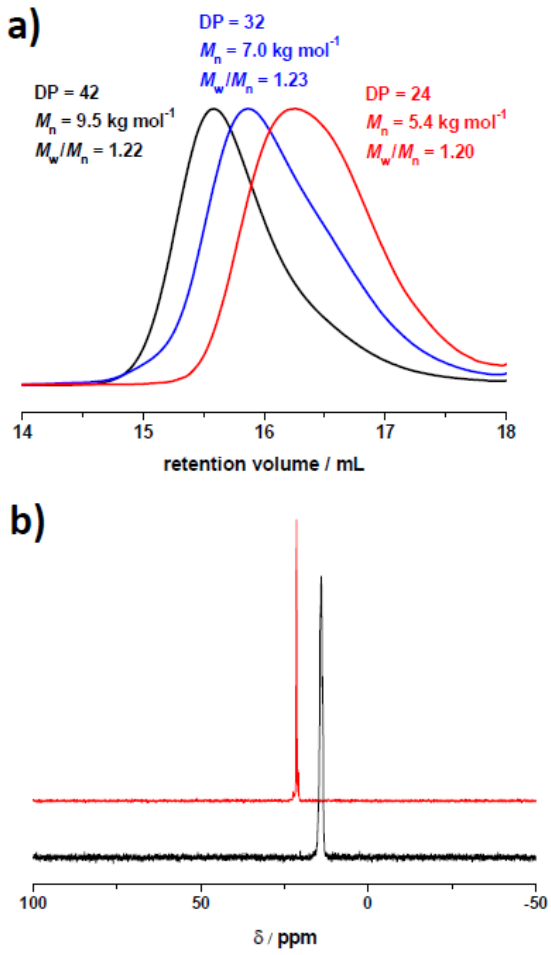

Figure 1. (a) DMF gel permeation chromatography traces obtained for the three PMP macro-CTAs used in this study. (b) ^{31}P NMR spectra recorded for the PMP_{24} macro-CTA before (red spectrum) and after hydrolysis (black spectrum). This indicates complete hydrolysis of the dimethyl ester groups on the PMP precursor to produce a well-defined PMPA macro-CTA.

Unfortunately, stable colloidal dispersions could not be obtained when targeting a PHPMA block with a degree of polymerization of 200 at 70 °C using ACVA initiator. This behavior was rather unexpected, as each of the PMP macro-CTAs exhibited excellent water solubility and no LCST-like behavior was observed. PISA syntheses were also attempted at 50 °C using AIBA as a

low temperature radical source,[63] but again precipitation was observed. Since we have recently developed various robust PISA formulations based on the RAFT alcoholic dispersion polymerization of BzMA,[48,49,54,55] we switched to using either ethanol or methanol as the continuous phase. However, coagulation was again obtained for the former solvent when targeting DPs of 200. It is perhaps noteworthy that complete dissolution of the steric stabilizer macro-CTA required stirring for around 1 h regardless of its molecular weight, which suggests that ethanol is perhaps a rather marginal solvent for PMP. Consequently, we selected methanol as a more polar solvent, which led to significantly faster PMP dissolution under the same conditions.

For kinetic studies of PISA syntheses conducted in methanol, an initial BzMA polymerization was conducted at 64 °C for 24 h at 20% w/w solids (see Scheme 1) using a PMP_{24} macro-CTA and targeting a final PBzMA block DP of 300. No precipitation was observed for this formulation, which produced a turbid dispersion. More than 99% conversion was attained after 24 h as judged by ^{1}H NMR studies, with almost complete monomer consumption (> 97%) being achieved within 13 h (Figure 2a). Moreover, an enhanced rate of polymerization is only observed relatively late in the polymerization – well after micellar nucleation has occurred (see inset in Figure 2a). This differs markedly from previous observations for similar PISA formulations based on RAFT alcoholic dispersion polymerization, where the increase in the rate of propagation coincides with the onset of micellar nucleation.[49,79] A tentative explanation for this observation might be the relatively small size of the spherical nanoparticles initially formed during this PISA formulation (D_h < 25 nm, see Table S1). This suggests the presence of rather loose, hydrated aggregates and thus perhaps relatively inefficient initial solubilization of the BzMA monomer within the nascent nuclei. For PISA syntheses conducted under appropriate conditions, the copolymer morphology is known to evolve from spheres to vesicles *via* various intermediate morphologies, including worms

and 'jellyfish'.[80] When the vesicle dimension (*i.e.* mean diameter and/or mean membrane thickness) reaches a certain critical value, these aggregates are able to solubilize BzMA. Thus, a significant increase in the rate of BzMA polymerization occurs at around 6 h, as seen in the third stage in the first order kinetics plot.

Despite this unusual kinetic behavior, the PISA formulation proved to be both efficient and reasonably well-controlled in terms of both copolymer morphology and molecular weight distribution. DLS studies of aliquots extracted during polymerization indicate that vesicles of around 160 nm are formed within 6 h, which suggests that the observed rate enhancement is associated with this morphology, rather than the initial spherical nuclei (see inset in Figure 2a and Table S1). These vesicles eventually attain a final hydrodynamic diameter of approximately 180 nm. A *post mortem* TEM image of the final copolymer morphology obtained after 24 h is shown in Figure S3b; the vesicular morphology is confirmed and the estimated mean vesicle diameter is in reasonably good agreement with the DLS studies. Given the non-ionic nature of the PMP macro-CTA used in this set of experiments, DMF-GPC analysis of the corresponding PMP_{24}-$PBzMA_x$ diblock copolymers was possible. Selected chromatograms are plotted in Figure 2b. The unimodal GPC traces are symmetric and show no significant tailing due to prematurely-terminated macro-CTA chains, indicating high blocking efficiencies. This is supported by the linear evolution of the number-average molecular weight, M_n, while maintaining relatively narrow molecular weight distributions, with M_w/M_n values typically below 1.16 (Figure S3a and Table S1). These observations are consistent with the anticipated pseudo-living character of this RAFT dispersion polymerization. In addition, a high molecular weight shoulder gradually becomes more prominent above 30% conversion. Similar observations were also reported for another alcoholic PISA formulation utilizing BzMA as the core-forming block.[49]

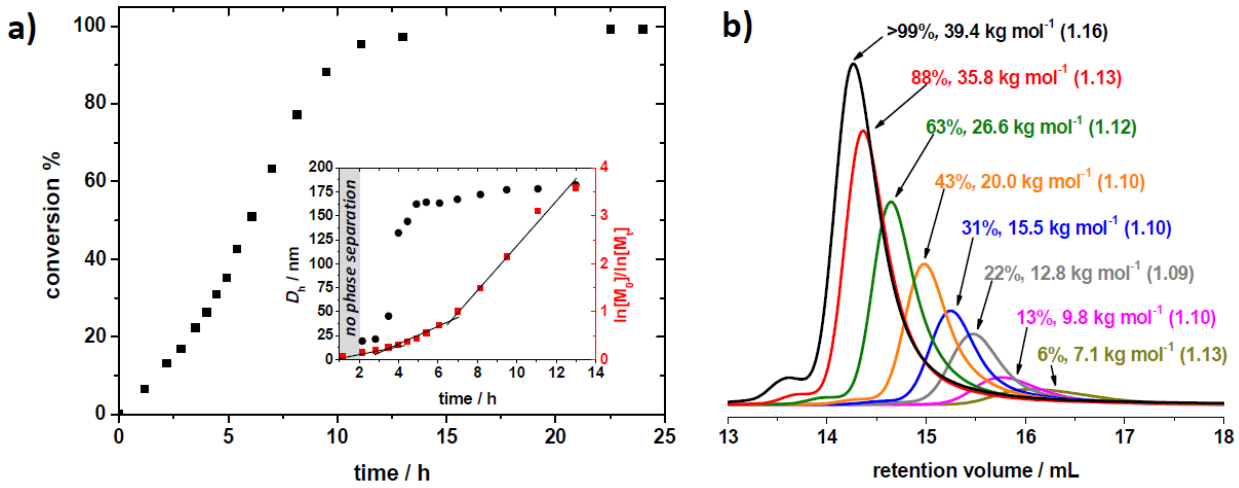

Figure 2. (a) Kinetic data derived from ^{1}H NMR studies of the RAFT alcoholic dispersion polymerization of BzMA (target DP = 300) at 64 °C using the PMP_{24} macro-CTA at 20% w/w solids in methanol. The inset shows the evolution of the hydrodynamic diameter D_h and the first order kinetic plot with respect to monomer. (b) The corresponding DMF GPC traces and the associated M_n and M_w/M_n data obtained for selected copolymers on sampling this formulation, indicating its reasonably good controlled/living character (see Table S1 for a more complete set of GPC data).

Using various PMP_x macro-CTAs (x = 24, 32, and 42) and performing all BzMA polymerizations at 20% w/w solids in methanol, we were able to construct a detailed phase diagram by systematically varying the target DP for the core-forming PBzMA block from 50 to 300 (see Figure 3; details of the individual polymerizations are provided in Table 1). The corresponding GPC traces for all of these PMP-PBzMA syntheses are shown in Figure S4 and clearly indicate an evolution of the molecular weight with increasing target PBzMA DP. High blocking efficiencies

and relatively low M_w/M_n values were obtained, where these are similar to the data discussed earlier for the kinetic study conducted when targeting PMP_{24}-$PBzMA_{300}$. However, a relatively low concentration of unreacted macro-CTA can be detected for the PMP_{42} macro-CTA, which suggests that some degree of premature termination occurred in this particular case. Moreover, the final molecular weight distribution was significantly broader (M_w/M_n = 1.53) for PMP_{42}-$PBzMA_{558}$ compared to all other polymerizations (M_w/M_n < 1.21). As discussed earlier, a high molecular weight shoulder becomes discernible when targeting PBzMA DPs greater than 100 for all PMP macro-CTAs. In previous studies involving a poly(2-hydroxypropyl methacrylate) core-forming block, a similar shoulder was explained in terms of a relatively low level of dimethacrylate impurity in the monomer, which inevitably leads to light branching when targeting higher DPs.[41] However, this explanation seems to be unlikely for benzyl methacrylate, since there is no reason for such a monomer to contain a dimethacrylate impurity. An alternative explanation may be some degree of termination by combination, which is not unknown for methacrylic monomers.[81]

Inspecting the phase diagram shown in Figure 3, it is clear that only spherical nanoparticles can be obtained when using the PMP_{42} macro-CTA. Presumably, this longer block confers additional steric stabilization during the BzMA polymerization and hence prevents sphere-sphere fusion, which is the key first step in the generation of worms and vesicles. Systematically increasing the target PBzMA DP from 50 to 558 leads to a monotonic increase in particle size, with hydrodynamic diameters ranging from 16 nm to 76 nm, as evidenced by both DLS and TEM (see Table 1 and Figure S5). The larger spheres are believed to be kinetically-trapped morphologies.[38]

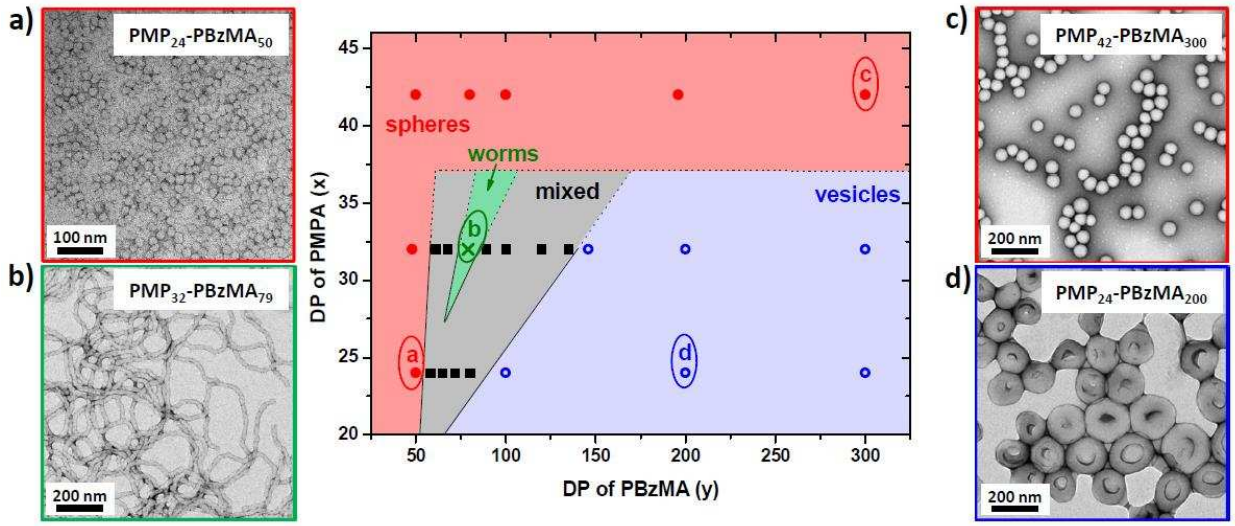

Figure 3. Phase diagram constructed for PMP_x-$PBzMA_y$ diblock copolymer nano-objects prepared in methanol at 64 °C at 20% w/w solids. Representative TEM images obtained for the three pure copolymer morphologies: (a) PMP_{24}-$PBzMA_{50}$ (small spheres), (b) PMP_{32}-$PBzMA_{79}$ (worms), (c) PMP_{42}-$PBzMA_{300}$ (large spheres), and (d) PMP_{24}-$PBzMA_{200}$ (vesicles).

We recently reported similar findings for a PHPMA-PBzMA RAFT alcoholic dispersion polymerization formulation, when employing a PHPMA macro-CTA with a DP of 63.[49] However, using shorter PMP stabilizer blocks (DP = 24 or 32) enables access to higher order morphologies, as well as spheres. Such rich phase behavior was also observed by Zehm and co-workers for the PHPMA-PBzMA PISA formulation on reducing the mean DP of the stabilizer block.[49] In the present study, using the PMP_{24} macro-CTA only enabled access to pure spheres, vesicles or mixed phases (Figure 3a and d). However, pure worms occupying a very narrow phase region could be obtained when employing the PMP_{32} macro-CTA (Figure 3b). Representative TEM images obtained for the entire PMP_{32}-$PBzMA_y$ series are shown in Figure S6. Increasing y from 48 to 61 led to partial fusion of spherical nanoparticles to form a mixture of spheres and short worms, with the latter having a distinctive 'pearl necklace' appearance. Increasing y by a further seven BzMA

units produced longer worms, with only a few spheres present. When y = 79, a free-standing gel comprising well-defined worms was obtained. Longer core-forming blocks (89 < y < 135) produced mixed phases, with vesicular phases becoming increasingly common. Finally, a pure vesicular phase was attained for PMP_{32}-$PBzMA_{146}$ (and higher y values). DLS studies suggest that increasing the DP of the PBzMA core induces some contraction in the mean vesicle dimensions (from D_h = 158 nm for y = 146 to D_h = 136 nm for y = 300). A similar size reduction was observed for the PMP_{24}-$PBzMA_y$ series, where y = 100 - 300, with hydrodynamic diameters decreasing from 352 nm to 181 nm (see Table 1). This may be caused by thickening of the vesicle membranes exclusively *via* inward growth.[82] TEM images recorded for the various PMP_{32}-$PBzMA_y$ PISA formulations provide some evidence for this hypothesis. For mixed phases consisting of worms and vesicles, the vesicle membrane is clearly visible and the vesicles are rather polydisperse (see Figure S6; y = 100, 120, and 135). On further increasing y, the vesicles become somewhat less polydisperse and their associated lumen volumes are reduced (see Figure S6; y = 146, 200 and 300). Minimization of the vesicular interfacial area (and hence free energy) is the driving force for this phenomenon, which was recently described in detail for an aqueous PISA formulation.[82] On the other hand, it is not yet understood why vesicles of apparently *increasing* diameter were observed after approximately 6 h during the kinetic studies (inset in Figure 2a).

Table 1. Summary of Monomer Conversions, Intensity-Average Particle Diameters, and GPC Data Obtained for a Series of Non-Ionic PMP_x-$PBzMA_y$ Diblock Copolymers Synthesized at 20% w/w Solids *via* RAFT Alcoholic Dispersion Polymerization of BzMA in Methanol at 64 °C for 24 h (S = Spheres, W = Worms, V = Vesicles).

target composition	BzMA % conv.	BzMA DP	GPC	DLS	TEM

			M_n [kg mol^{-1}]	M_w/M_n	D_h	PDI	morphology
PMP_{24}-$PBzMA_{50}$	99	50	9.8	1.17	24	0.29	S
PMP_{24}-$PBzMA_{58}$	99	57	11.0	1.15	35	0.43	S+W
PMP_{24}-$PBzMA_{65}$	>99	65	11.7	1.15	812	0.99	S+W
PMP_{24}-$PBzMA_{72}$	>99	72	12.4	1.15	312	0.55	S+W+V
PMP_{24}-$PBzMA_{80}$	>99	80	13.3	1.14	238	0.30	W+V
PMP_{24}-$PBzMA_{100}$	>99	100	15.8	1.14	352	0.12	V
PMP_{24}-$PBzMA_{200}$	>99	200	28.1	1.11	201	0.20	V
PMP_{24}-$PBzMA_{300}$	>99	300	34.7	1.21	181	0.07	V
PMP_{32}-$PBzMA_{50}$	96	48	10.6	1.19	17	0.09	S
PMP_{32}-$PBzMA_{65}$	94	61	12.0	1.20	29	0.26	S+W
PMP_{32}-$PBzMA_{70}$	97	68	12.6	1.17	84	0.28	S+W
PMP_{32}-$PBzMA_{80}$	99	79	13.7	1.18	249	0.31	W
PMP_{32}-$PBzMA_{90}$	99	89	14.4	1.19	499	0.47	W+V
PMP_{32}-$PBzMA_{100}$	>99	100	16.0	1.15	356	0.44	W+V
PMP_{32}-$PBzMA_{120}$	>99	120	19.3	1.16	167	0.09	W+V
PMP_{32}-$PBzMA_{135}$	>99	135	20.6	1.18	175	0.17	W+V
PMP_{32}-$PBzMA_{150}$	97	146	22.5	1.15	158	0.07	V
PMP_{32}-$PBzMA_{200}$	>99	200	27.7	1.16	152	0.03	V
PMP_{32}-$PBzMA_{300}$	>99	300	39.2	1.20	136	0.03	V
PMP_{42}-$PBzMA_{50}$	>99	50	14.7	1.18	16	0.16	S
PMP_{42}-$PBzMA_{80}$	>99	80	22.7	1.17	23	0.12	S
PMP_{42}-$PBzMA_{100}$	>99	100	25.9	1.18	27	0.13	S
PMP_{42}-$PBzMA_{200}$	98	196	44.1	1.17	53	0.08	S
PMP_{42}-$PBzMA_{300}$	>99	300	63.1	1.19	63	0.11	S
PMP_{42}-$PBzMA_{600}$	93	558	109.5	1.53	76	0.06	S

We then examined the use of anionic PMPA macro-CTAs as putative steric stabilizers for the RAFT aqueous dispersion polymerization of HPMA. According to Semsarilar and co-workers, strong electrostatic repulsion between adjacent polyelectrolytic stabilizer blocks can impede *in situ* self-assembly during attempted aqueous PISA syntheses.[66-68] We investigated this hypothesis for our system by targeting a HPMA DP of 300; such an asymmetric diblock copolymer might be expected to form vesicles. However, it proved impossible to obtain pure vesicles for various PISA

formulations at pH 5, even when utilizing binary mixtures of non-ionic poly(glycerol monomethacrylate) ($PGMA_{45}$) with an anionic $PMPA_x$ macro-CTA in the presence of added salt to screen the unfavorable electrostatics. Table S2 and Figure S7 summarize this series of experiments, for which a detailed protocol is given in the Supporting Information.

In view of these negative results, RAFT alcoholic dispersion polymerization of BzMA was performed in methanol at 20% w/w solids using each of the PMPA macro-CTAs in turn (see Scheme 1). For this series of experiments, it was envisaged that the significantly lower dielectric constant of methanol (ε = 32.6 at 298 K) compared to water (ε = 78.5 at 298K)[83] might reduce the unfavorable electrostatic repulsive forces and hence facilitate PISA. A PMPA macro-CTA with a mean DP of 24 was chosen for a kinetic study of the dispersion polymerization of BzMA at 64 °C. When targeting a DP of 300 for the PBzMA block, greater than 99% conversion was achieved after 24 h, as judged by ^{1}H NMR (Figure 4a). A significant rate enhancement was observed, again not at the onset of micellar nucleation but instead when spherical micelles first begin to fuse to form higher order morphologies (see inset in Figure 4a). The apparent first-order rate constant, k_{app}, for this second stage was a little higher when using the anionic $PMPA_{24}$ stabilizer (k_{app} = 8.4 x 10^{-5} s^{-1}) compared to the non-ionic PMP_{24} macro-CTA (k_{app} = 5.5 x 10^{-5} s^{-1}). This suggests higher partitioning of the non-polar BzMA monomer within the growing micelle cores in the former case. DLS data are shown for all samples in Figure 4a (see inset) and summarized in Table S3. A representative TEM image of the final vesicular morphology is depicted in Figure 4b: the estimated mean vesicle diameter of approximately 510 nm (based on analysis of 80 particles) is in reasonably good agreement with that indicated by DLS, bearing in mind that the latter technique reports a hydrodynamic diameter and is biased towards larger particles.

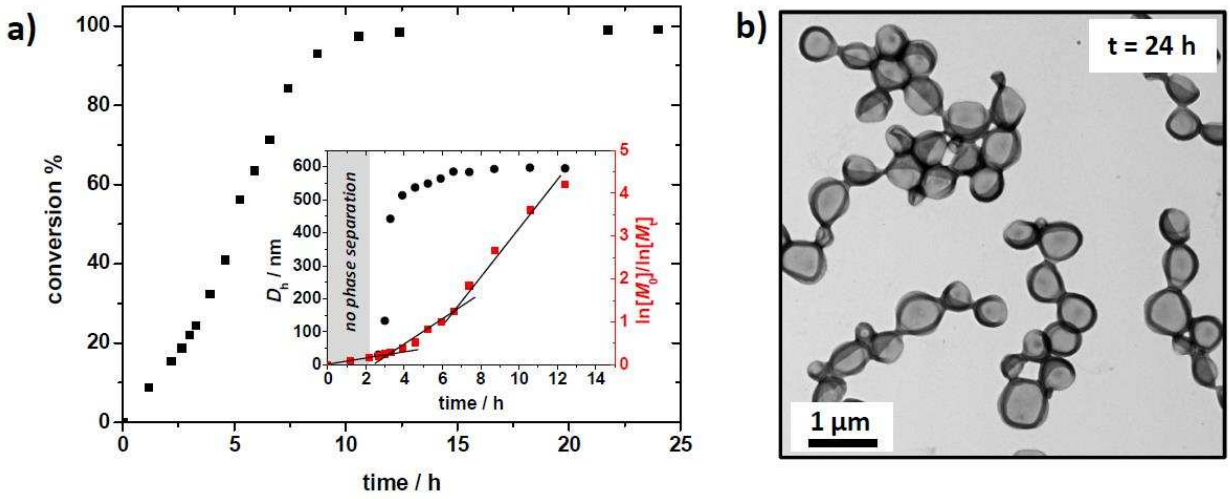

Figure 4. (a) Kinetic data derived from ^{1}H NMR studies of the RAFT alcoholic dispersion polymerization of BzMA (target DP = 300) using an anionic $PMPA_{24}$ macro-CTA at 20% w/w solids in methanol at 64 °C. The inset shows the evolution of the hydrodynamic diameter D_h and the first order kinetic plot with respect to monomer concentration. (b) Representative TEM image of the final vesicular morphology obtained after 24 h (> 99% conversion).

Unfortunately, DMF GPC analysis of the various PMP_{24}-$PBzMA_y$ diblock copolymers was not feasible because of unfavorable copolymer-column interactions. Moreover, the hydrophobic character of the PBzMA block precluded aqueous GPC analysis. In view of these problems, chain extension experiments were conducted for each of the three PMPA macro-CTAs in turn using GMA to produce a water-soluble PGMA block, simply in order to assess blocking efficiencies when polymerizing a second methacrylic monomer. Aqueous GPC traces obtained for these $PMPA_x$-$PGMA_y$ diblock copolymers are compared to the respective PMPA macro-CTAs in Figure S1. In each case symmetric monomodal curves were obtained, with pronounced shifts to higher molecular weight relative to the original PMPA macro CTA. All three PMPA-PGMA diblock

copolymers exhibited relatively narrow molecular weight distributions (M_w/M_n < 1.07). This indicates high blocking efficiencies for the solution polymerization of GMA. Given that the pseudo-living character of RAFT dispersion polymerization is enhanced compared to solution polymerization,[84] at least comparable (and most likely higher) blocking efficiencies are anticipated under the former conditions.

Using the three PMPA macro-CTAs (DP = 24, 32 or 42) to target a range of core-forming PBzMA blocks enables the construction of a predictive phase diagram (Figure 5). A summary of the individual PISA syntheses conducted at 20% w/w solids in methanol at 64 °C is shown in Table 2. In contrast to the phase diagram for the PMP-PBzMA formulation, non-spherical morphologies can be observed even for the $PMPA_{42}$ macro-CTA. At first sight, this might seem surprising given the anionic nature of the stabilizer chains, which might be expected to impede fusion of the initial spheres (and indeed hinder PISA itself).[67,68] However, electrostatic repulsive forces are substantially reduced in methanol compared to aqueous media. This hypothesis is consistent with the results obtained for the corresponding PMPA-PHPMA aqueous PISA formulations (see table S2), which do not readily provide access to pure copolymer phases even when employing binary mixtures of anionic and non-ionic macro-CTAs. The phase diagram for the $PMPA_x$-$PBzMA_y$ formulations shown in Figure 5 contains a relatively broad vesicle phase and a somewhat narrower mixed phase region.

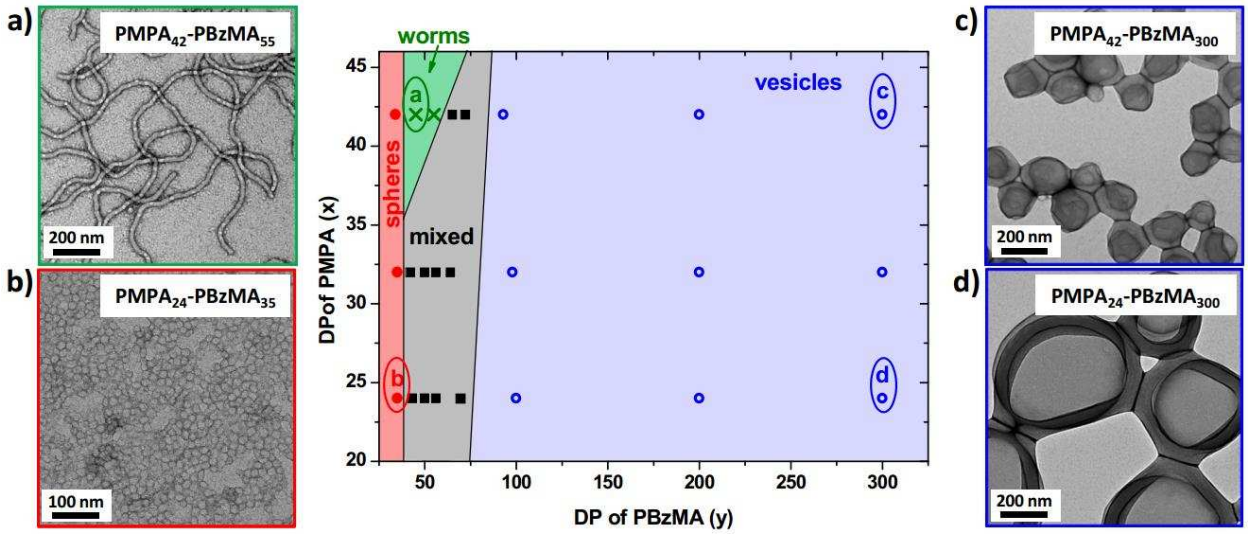

Figure 5. Phase diagram constructed for $PMPA_x$-$PBzMA_y$ diblock copolymer nano-objects prepared in methanol at 64 °C at 20% w/w solids. TEM images for pure copolymer morphologies: (a) $PMPA_{42}$-$PBzMA_{55}$ (worms), (b) $PMPA_{24}$-$PBzMA_{35}$ (spheres), (c) $PMPA_{42}$-$PBzMA_{300}$ (small vesicles), and (d) $PMPA_{24}$-$PBzMA_{300}$ (large vesicles).

Spheres are accessible up to a target PBzMA DP of 35 (Figure 5b), while pure worms can only be obtained when using the $PMPA_{42}$ macro-CTA (Figure 5a). Furthermore, the *anionic* $PMPA_{24}$-$PBzMA_{300}$ vesicles shown in Figure 5d (D_h from DLS = 529 nm) are significantly larger than the corresponding *non-ionic* PMP_{24}-$PBzMA_{300}$ vesicles (D_h from DLS = 181 nm). In principle, a higher packing parameter might be expected to favor the formation of larger vesicles.[85] This therefore suggests that the hydrodynamic volume occupied by an anionic $PMPA_{24}$ chain in methanol is less than that of a non-ionic PMP_{24} chain, indicating reduced solvation of the former stabilizer under these conditions. Similarly, increasing the PMPA stabilizer DP for a given core-forming PBzMA DP reduces the mean vesicle dimensions, presumably because of the larger hydrodynamic volume occupied by the PMPA chains (Figure 5c). The $PMPA_{42}$-$PBzMA_y$ series provides access to all three copolymer morphologies, with representative TEM images being

shown in Figure S8. As for the non-ionic PMP-PBzMA formulations, there is an apparent reduction in vesicle dimensions when targeting higher degrees of polymerization of the PBzMA block and these observations are supported by DLS studies (see corresponding entries in Table 2).

Generation of Organic-Inorganic Hybrid Materials. It is well recognized that naturally occurring biopolymers are intimately involved in the formation of biominerals,[86] where these can not only direct features such as polymorph and morphology, but also enhance mechanical properties through occlusion within the crystal lattice.[87,88] Importantly, this behavior is not restricted to biomacromolecules and recent work has shown that a range of additives, including sub-micron latex particles, various anionic diblock copolymer nano-objects, and even small molecules can become occluded within single crystals of calcite ($CaCO_3$).[89-94] In all cases, successful occlusion is dependent on the additives binding to the surfaces of the growing crystals, but remaining dispersed in the crystal growth solution.[92] The PMPA-PBzMA nano-objects synthesized here provide interesting candidates for controlling $CaCO_3$ precipitation. Both phosphate and phosphonic acid functionalized surfactants and polymers are well known to interact strongly with $CaCO_3$, and are widely used as crystal growth inhibitors.[95,96] The efficiency of occlusion of these additives within calcite was therefore investigated, and the results compared with the corresponding non-ionic PMP-PBzMA nano-objects.

Table 2. Summary of Monomer Conversions and Intensity-Average Particle Diameters Obtained for a Series of Anionic $PMPA_x$-$PBzMA_y$ Diblock Copolymers Conducted at 20% w/w Solids *via* RAFT Alcoholic Dispersion Polymerization in Methanol at 64 °C for 24 h (S = Spheres, W = Worms, L = Lamellae and V = Vesicles).

target composition	BzMA % conv.	BzMA DP	DLS		TEM
			D_h	PDI	morphology
$PMPA_{24}$-$PBzMA_{35}$	>99	35	15	0.13	S
$PMPA_{24}$-$PBzMA_{45}$	96	43	61	0.29	S+W
$PMPA_{24}$-$PBzMA_{50}$	>99	50	421	0.61	S+W+V
$PMPA_{24}$-$PBzMA_{60}$	94	56	556	0.29	S+L+V
$PMPA_{24}$-$PBzMA_{70}$	>99	70	429	0.91	S+L+V
$PMPA_{24}$-$PBzMA_{100}$	>99	100	459	0.18	V
$PMPA_{24}$-$PBzMA_{200}$	>99	200	439	0.14	V
$PMPA_{24}$-$PBzMA_{300}$	>99	300	529	0.06	V
$PMPA_{32}$-$PBzMA_{35}$	>99	35	17	0.10	S
$PMPA_{32}$-$PBzMA_{42}$	96	40	38	0.23	S+W
$PMPA_{32}$-$PBzMA_{50}$	>99	50	227	0.57	S+W
$PMPA_{32}$-$PBzMA_{56}$	>99	56	517	0.68	W+L+V
$PMPA_{32}$-$PBzMA_{70}$	91	64	405	0.16	W+V
$PMPA_{32}$-$PBzMA_{72}$	>99	72	355	0.24	W+V
$PMPA_{32}$-$PBzMA_{100}$	98	98	309	0.23	V
$PMPA_{32}$-$PBzMA_{200}$	>99	200	282	0.14	V
$PMPA_{32}$-$PBzMA_{300}$	>99	300	212	0.07	V
$PMPA_{42}$-$PBzMA_{35}$	98	34	21	0.08	S
$PMPA_{42}$-$PBzMA_{50}$	90	45	174	0.29	W
$PMPA_{42}$-$PBzMA_{55}$	>99	55	267	0.29	W
$PMPA_{42}$-$PBzMA_{70}$	93	65	248	0.22	W+V
$PMPA_{42}$-$PBzMA_{72}$	>99	72	246	0.21	W+V
$PMPA_{42}$-$PBzMA_{100}$	93	93	194	0.16	V
$PMPA_{42}$-$PBzMA_{200}$	>99	200	264	0.10	V
$PMPA_{42}$-$PBzMA_{300}$	>99	300	214	0.02	V

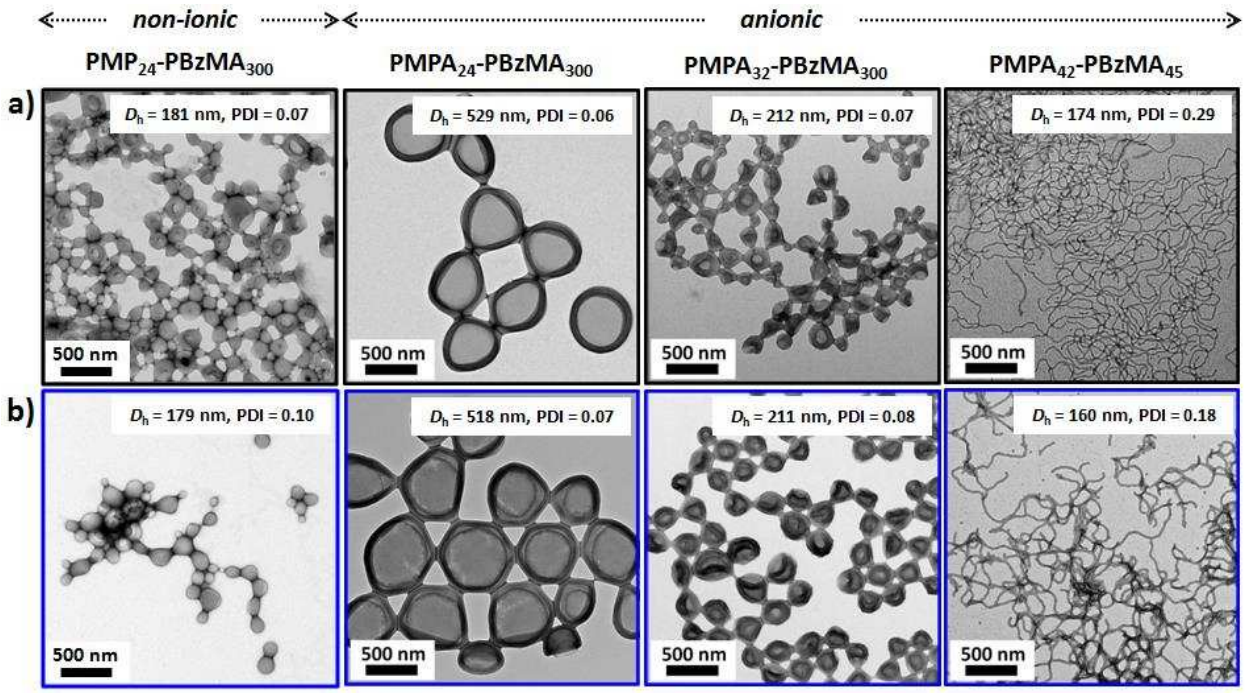

Figure 6. (a) Representative TEM images recorded for *non-ionic* PMP_{24}-$PBzMA_{300}$ vesicles and *anionic* $PMPA_x$-$PBzMA_y$ worms and vesicles, obtained *via* RAFT dispersion polymerization of BzMA at 20% w/w solids in methanol at 64 °C. (b) TEM images for the same copolymer nanoparticles after their transfer from methanol to water *via* exhaustive dialysis at 20 °C. In all cases the copolymer concentration used to prepare the TEM grids was 0.2% w/w.

The nano-objects were first transferred from the methanol continuous phase to water *via* dialysis. TEM analysis of selected nano-objects before and after dialysis indicated no adverse effect on the copolymer morphology (Figure 6), where these findings were supported by DLS studies which showed no change in the mean particle diameter before and after dialysis. These observations are consistent with the relatively high T_g of around 55 °C for the core-forming PBzMA block, which suppresses exchange of copolymer chains between kinetically-frozen nano-objects. In addition to the successful transfer of vesicles into aqueous media ($PMPA_{32}$-$PBzMA_{300}$, $PMPA_{24}$-$PBzMA_{300}$,

and PMP_{24}-$PBzMA_{300}$), an aqueous worm dispersion was also obtained after dilution of a methanolic worm gel followed by dialysis ($PMPA_{42}$-$PBzMA_{45}$, see Figure 6). Aqueous electrophoresis studies of these anionic nano-objects confirmed highly anionic zeta-potentials of -35 to -45 mV across a wide pH range (see Figure 7). Only in relatively acidic media (pH 2) was a modest reduction in zeta potential observed, as expected for a steric stabilizer based on a strong polyacid such as PMPA. Concomitant DLS studies indicated no significant change in particle dimensions from pH 2 to 10, suggesting that colloidal stability was maintained, see Figure 7.

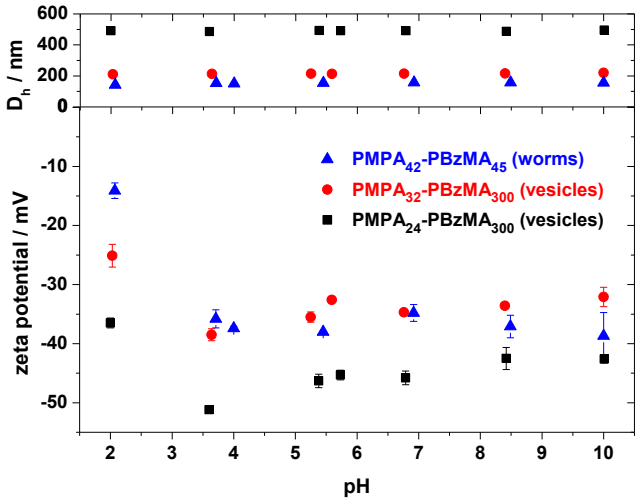

Figure 7. Aqueous electrophoresis curves and DLS data obtained for $PMPA_x$-$PBzMA_y$ worms and vesicles prepared by RAFT alcoholic dispersion polymerization of BzMA in methanol at 20% w/w solids. Measurements were conducted using 0.01% w/v dispersions in the presence of 10 mM NaCl as background electrolyte.

Occlusion experiments were conducted by precipitating $CaCO_3$ in the presence of *non-ionic* PMP_{24}-$PBzMA_{300}$ vesicles and the various *anionic* $PMPA_x$-$PBzMA_y$ nano-objects at pH ≈ 9 *via* a

one-pot protocol using the ammonia diffusion method.[78] All experiments were conducted using a fixed stock solution of 1.5 mM $CaCl_2$ and a copolymer concentration of either 0.010% w/w (Figure 8a) or 0.005% w/w (Figure 8b). All dispersions remained colloidally stable in the presence of the $CaCl_2$ solution, which was added at an initial pH of less than 6. Rhombohedral calcite crystals of 10 to 15 μm were prepared in control experiments performed in the absence of diblock copolymer nano-objects. Figure S9 shows a typical Raman spectrum recorded for calcite crystals grown under these conditions, with the characteristic calcite bands being observed at 155 and 282 (lattice modes), 710 (v_4) and 1085 cm^{-1}(v_1).[92] Formation of calcite in the presence of *non-ionic* PMP_{24}-$PBzMA_{300}$ vesicles at both additive concentrations produced crystals with comparable habits and dimensions to those formed in the control experiments. SEM studies confirmed that the crystals were perfect rhombohedra with well-defined edges, with just a few weakly interacting vesicles located on the crystal surface. These findings were not unexpected, since anionic character is believed to be a pre-requisite for successful occlusion. Raman microscopy studies of such crystals formed when using 0.010% w/w copolymer confirmed that the polymorph was indeed calcite (Figure S9).

In contrast, the *anionic* nano-objects had a stronger influence on the morphology and dimensions of the calcite crystals. Well-defined rhombohedral crystals of 15 to 20 μm were formed in the presence of 0.005% w/w $PMPA_{24}$-$PBzMA_{300}$ and $PMPA_{32}$-$PBzMA_{300}$ vesicles (DLS studies indicated mean diameters of approximately 520 nm and 210 nm, respectively). At the higher copolymer concentration, 20 to 25 μm crystals with increasingly rough faces and edge truncations were obtained.

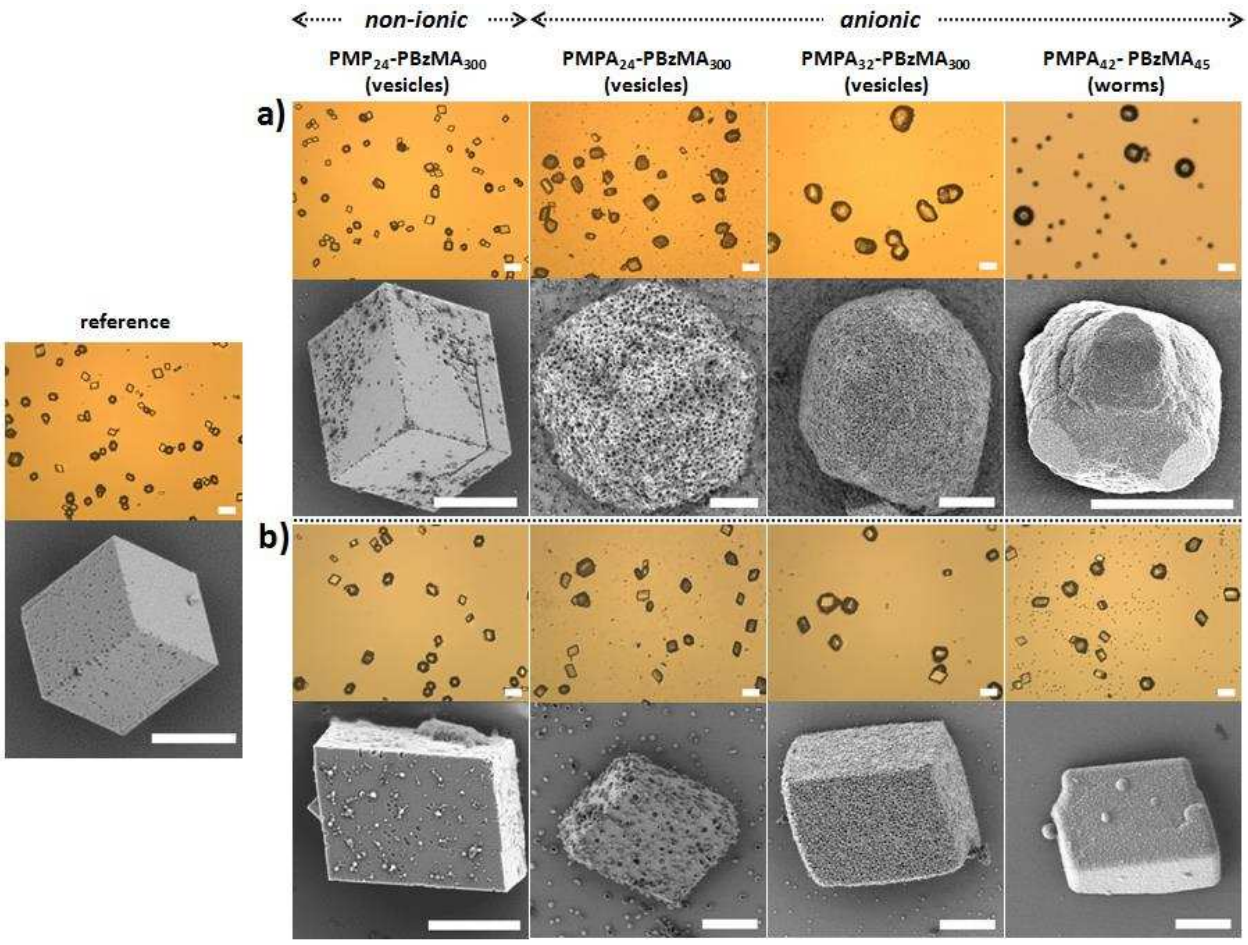

Figure 8. Optical micrographs and corresponding SEM images obtained for a series of $CaCO_3$ crystals prepared using a 1.5 mM $CaCl_2$ solution and either (a) 0.010% w/w or (b) 0.005% w/w PMPA-PBzMA or PMP- PBzMA diblock copolymer nano-objects. The scale bar corresponds to 20 μm and 5μm for the optical micrographs and SEM images, respectively. Optical micrograph and SEM images of the reference calcite crystals precipitated in the absence of diblock copolymer nano-objects are shown at the left-hand side.

Again, Raman studies indicated calcite formation under these conditions (Figure S9). Anionic $PMPA_{42}$-$PBzMA_{45}$ worms had an even more pronounced effect, generating a bimodal distribution of small ~ 7 μm calcite crystals and larger ~ 20 μm polycrystalline vaterite particles at a copolymer

concentration of 0.010% w/w, as confirmed by Raman microscopy (see Figure S9). At an additive concentration of 0.050% w/w, copolymer overgrown calcite rhombohedra with somewhat curved edges and roughened faces are produced. This indicates a strong interaction between the anionic nano-objects and the crystal lattice.

The crystals were also fractured to give a rough estimate of the relative degrees of occlusion of these contrasting nano-objects. Figure 9 shows both intact and fractured crystals prepared at the two different additive concentrations. The *non-ionic* PMP_{24}-$PBzMA_{300}$ vesicles are not occluded at all, whereas a moderate degree of occlusion can be observed for both $PMPA_{32}$-$PBzMA_{300}$ and $PMPA_{24}$-$PBzMA_{300}$ *anionic* vesicles. This is particularly interesting for the latter vesicles, which have mean diameters of ~520 nm, and are thus significantly larger than the occluded 200 nm latex particles occluded in earlier work.[94] These vesicles are of potential interest as carriers of functional additives. However, the degree of vesicle occlusion appears to be significantly higher at the periphery of the crystals for both additive concentrations. This may derive from an increase in incorporation efficiency at the lower supersaturation encountered towards the end of the crystallization experiments[78] or could suggest a mass-transport limited crystallization mechanism in which vesicle diffusion to the surface of the growing calcite crystals limits occlusion. This would again promote occlusion during the later, slower stages of growth. In contrast, the ~ 200 nm anionic $PMPA_{32}$-$PBzMA_{300}$ vesicles, are incorporated to much greater extents at both polymer concentrations. Furthermore, homogeneous occlusion throughout the crystal is observed. This suggests that the incorporation of larger particles may be more dependent on the reaction conditions, and in particular supersaturation, than that of smaller particles. Finally, examination of the distribution of the $PMPA_{42}$-$PBzMA_{45}$ worms within the crystals precipitated at the lower polymer concentration showed that they were predominantly located in the outer 1 μm region of

the crystal. In contrast, for the small calcite crystals precipitated at the higher additive concentration then worms appear to be occluded rather more homogeneously throughout the crystal.

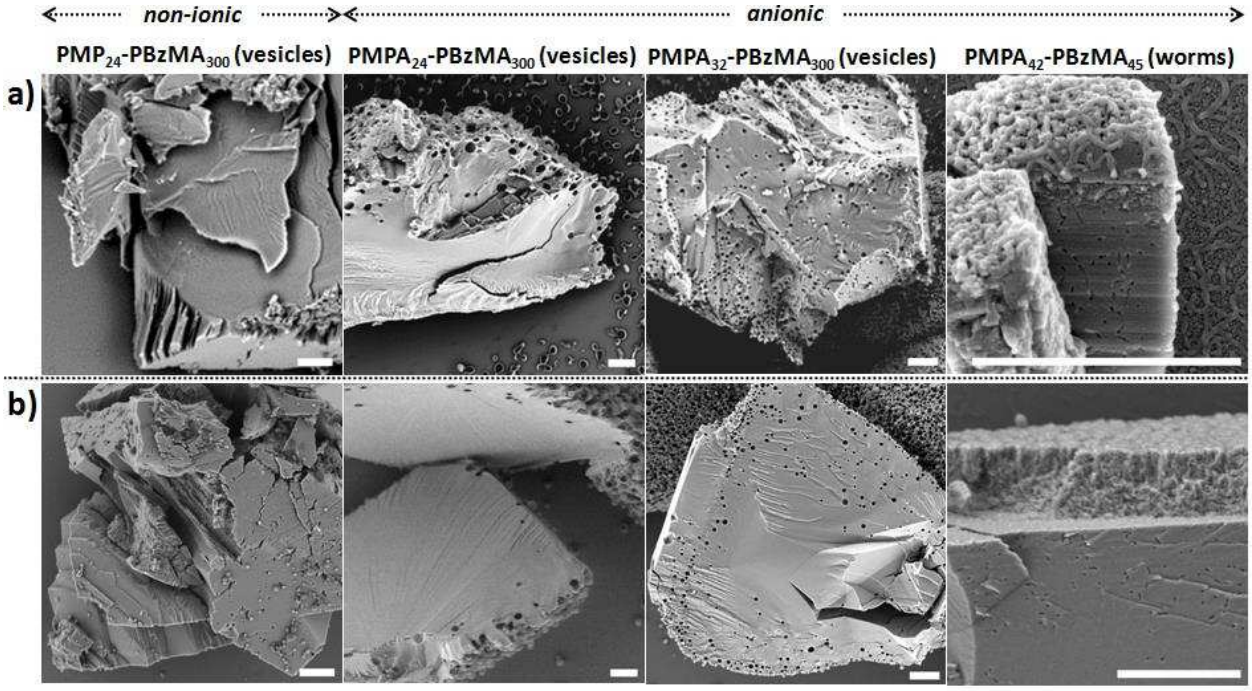

Figure 9. SEM images obtained for a series of fractured $CaCO_3$ crystals, prepared using a 1.5 mM $CaCl_2$ solution and (a) 0.010% w/w or (b) 0.005% w/w PMPA- or PMP-stabilized PBzMA diblock copolymer nano-objects. The scale bar represents 1.5 μm in all SEM images.

CONCLUSIONS

A new PISA formulation has been explored for the generation of both phosphonate- and phosphonic acid-stabilized spheres, worms and vesicles. More specifically, three poly(methacryloyloxymethyl dimethylphosphonate) [PMP] macro-CTAs with mean degrees of

polymerization of 24, 32, and 42 were synthesized *via* RAFT solution polymerization and converted into the corresponding poly(methacryloxymethyl phosphonic acid) [PMPA] macro-CTAs *via* ester hydrolysis. Subsequent chain extension with BzMA *via* RAFT methanolic dispersion polymerization at 20% w/w solids enabled construction of detailed phase diagrams for both types of macro-CTAs. Systematic variation of the target degree of polymerization of the PBzMA provides access to diblock copolymer spheres, worms and vesicles, as well as mixed phases. Comparing the performance of the same macro-CTA in its *non-ionic* and *anionic* forms allowed the effect of stabilizer charge density on self-assembly in non-aqueous media (*i.e.* methanol) to be assessed for the first time. GPC studies indicate high blocking efficiencies and low final polydispersities for all non-ionic PMP_x-$PBzMA_y$ diblock copolymers. However, for the anionic $PMPA_x$ macro-CTAs, blocking efficiencies could only be assessed indirectly *via* chain extension experiments conducted using a water-soluble monomer (glycerol monomethacrylate) as the second block. Transfer of selected diblock copolymer nano-objects from methanol to water *via* dialysis did not result in any discernible changes in copolymer morphology, as judged by TEM and DLS. Aqueous electrophoresis studies confirmed the highly anionic character of the phosphonic acid-stabilized nano-objects in aqueous media. Examination of both sets of copolymer nano-objects as crystal growth additives showed that *anionic* worms and vesicles were occluded within calcite crystals during the crsytal growth, while the corresponding *non-ionic* phosphonate-stabilized vesicles were not. These findings emphasize the importance of appropriate surface chemistry in promoting occlusion of organic nanoparticles within inorganic host crystals.

ASSOCIATED CONTENT

Supporting Information. ^{31}P NMR spectra and GPC data for the three PMPA macro-CTAs, GPC and DLS data for kinetics of dispersion polymerization experiments, GPC data for all PMP_x-$PBzMA_y$ diblock copolymers, additional TEM images, DLS data for aqueous dispersion polymerizations conducted using binary mixtures of macro-CTAs, and Raman spectra for selected $CaCO_3$ occlusion experiments. This material is available free of charge *via* the Internet at http://pubs.acs.org

AUTHOR INFORMATION

Corresponding Author

*E-mail s.p.armes@sheffield.ac.uk

ACKNOWLEDGMENTS

EPSRC is acknowledged for postdoctoral support of A.H. (grant EP/K006290/1) and A.N.K. (EP/K006304/1). The authors thank André H. Gröschel for the preparation of the nano-object illustrations.

REFERENCES

1. Lupa, L.; Popa, A.; Ilia, G. In *Phosphorus-Based Polymers: From Synthesis to Applications*; The Royal Society of Chemistry: 2014, p 225-251.
2. Clearfield, A. *Curr. Opin. Solid State Mater. Sci.* **2002**, *6*, 495-506.
3. van den Brand, J.; Van Gils, S.; Beentjes, P. C. J.; Terryn, H.; Sivel, V.; de Wit, J. H. W. *Prog. Org. Coat.* **2004**, *51*, 339-350.
4. Zhang, Q. M.; Serpe, M. J. *Macromolecules* **2014**, *47*, 8018–8025.
5. Alexandrino, E. M.; Ritz, S.; Marsico, F.; Baier, G.; Mailander, V.; Landfester, K.; Wurm, F. R. *J. Mater. Chem. B* **2014**, *2*, 1298-1306.
6. Brunklaus, G.; Schauff, S.; Markova, D.; Klapper, M.; Müllen, K.; Spiess, H.-W. *J. Phys. Chem. B* **2009**, *113*, 6674-6681.
7. Quittmann, U.; Lecamp, L.; El Khatib, W.; Youssef, B.; Bunel, C. *Macromol. Chem. Phys.* **2001**, *202*, 628-635.

8. Canadell, J.; Hunt, B. J.; Cook, A. G.; Mantecón, A.; Cádiz, V. *Polym. Degrad. Stab.* **2007**, *92*, 1482-1490.
9. Köppl, T.; Brehme, S.; Pospiech, D.; Fischer, O.; Wolff-Fabris, F.; Altstädt, V.; Schartel, B.; Döring, M. *J. Appl. Polym. Sci.* **2013**, *128*, 3315-3324.
10. Monge, S.; Canniccioni, B.; Graillot, A.; Robin, J.-J. *Biomacromolecules* **2011**, *12*, 1973-1982.
11. Lin, Z.; Cao, S.; Chen, X.; Wu, W.; Li, J. *Biomacromolecules* **2013**, *14*, 2206-2214.
12. David, G.; Asri, Z. E.; Rich, S.; Castignolles, P.; Guillaneuf, Y.; Lacroix-Desmazes, P.; Boutevin, B. *Macromol. Chem. Phys.* **2009**, *210*, 631-639.
13. Canniccioni, B.; Monge, S.; David, G.; Robin, J.-J. *Polym. Chem.* **2013**, *4*, 3676-3685.
14. Graillot, A.; Monge, S.; Faur, C.; Bouyer, D.; Robin, J.-J. *Polym. Chem.* **2013**, *4*, 795-803.
15. Grøndahl, L.; Suzuki, S.; Wentrup-Byrne, E. *Chem. Commun.* **2008**, 3314-3316.
16. Miyatake, K.; Hay, A. S. *J. Polym. Sci. A Polym. Chem.* **2001**, *39*, 1854-1859.
17. Watson, J. D.; Crick, F. H. C. *Nature* **1974**, *248*, 765-765.
18. Ornelas-Megiatto, C.; Wich, P. R.; Fréchet, J. M. J. *J. Am. Chem. Soc.* **2012**, *134*, 1902-1905.
19. Uchiyama, T.; Kiritoshi, Y.; Watanabe, J.; Ishihara, K. *Biomaterials* **2003**, *24*, 5183-5190.
20. Pegoraro, C.; Cecchin, D.; Gracia, L. S.; Warren, N.; Madsen, J.; Armes, S. P.; Lewis, A.; MacNeil, S.; Battaglia, G. *Cancer Lett.* **2013**, *334*, 328-337.
21. Hemp, S. T.; Smith, A. E.; Bryson, J. M.; Allen, M. H.; Long, T. E. *Biomacromolecules* **2012**, *13*, 2439-2445.
22. Liu, G.; Jin, Q.; Liu, X.; Lv, L.; Chen, C.; Ji, J. *Soft Matter* **2011**, *7*, 662-669.
23. Matyjaszewski, K. *Macromolecules* **2012**, *45*, 4015-4039.
24. Moad, G.; Rizzardo, E.; Thang, S. H. *Aust. J. Chem.* **2012**, *65*, 985-1076.
25. Lobb, E. J.; Ma, I.; Billingham, N. C.; Armes, S. P.; Lewis, A. L. *J. Am. Chem. Soc.* **2001**, *123*, 7913-7914.
26. Madsen, J.; Canton, I.; Warren, N. J.; Themistou, E.; Blanazs, A.; Ustbas, B.; Tian, X.; Pearson, R.; Battaglia, G.; Lewis, A. L.; Armes, S. P. *J. Am. Chem. Soc.* **2013**, *135*, 14863-14870.
27. Yusa, S.-i.; Fukuda, K.; Yamamoto, T.; Ishihara, K.; Morishima, Y. *Biomacromolecules* **2005**, *6*, 663-670.
28. Ohno, S.; Hasegawa, S.; Liu, H.; Ishihara, K.; Yusa, S.-i. *Polym J* **2014**.
29. Huang, J.; Matyjaszewski, K. *Macromolecules* **2005**, *38*, 3577-3583.
30. Suzuki, S.; Whittaker, M. R.; Grøndahl, L.; Monteiro, M. J.; Wentrup-Byrne, E. *Biomacromolecules* **2006**, *7*, 3178-3187.
31. Blidi, I.; Geagea, R.; Coutelier, O.; Mazieres, S.; Violleau, F.; Destarac, M. *Polym. Chem.* **2012**, *3*, 609-612.
32. Markova, D.; Kumar, A.; Klapper, M.; Müllen, K. *Polymer* **2009**, *50*, 3411-3421.
33. David, G.; Negrell, C.; Manseri, A.; Boutevin, B. *J. Appl. Polym. Sci.* **2009**, *114*, 2213-2220.
34. Charleux, B.; Delaittre, G.; Rieger, J.; D'Agosto, F. *Macromolecules* **2012**, *45*, 6753-6765.
35. Warren, N. J.; Armes, S. P. *J. Am. Chem. Soc.* **2014**, *136*, 10174-10185.
36. Sun, J.-T.; Hong, C.-Y.; Pan, C.-Y. *Polym. Chem.* **2013**, *4*, 873-881.
37. Cunningham, V. J.; Alswieleh, A. M.; Thompson, K. L.; Williams, M.; Leggett, G. J.; Armes, S. P.; Musa, O. M. *Macromolecules* **2014**, *47*, 5613-5623.
38. Blanazs, A.; Ryan, A. J.; Armes, S. P. *Macromolecules* **2012**, *45*, 5099-5107.

39. An, Z.; Shi, Q.; Tang, W.; Tsung, C.-K.; Hawker, C. J.; Stucky, G. D. *J. Am. Chem. Soc.* **2007**, *129*, 14493-14499.
40. Rieger, J.; Grazon, C.; Charleux, B.; Alaimo, D.; Jérôme, C. *J. Polym. Sci. A Polym. Chem.* **2009**, *47*, 2373-2390.
41. Li, Y.; Armes, S. P. *Angew. Chem. Int. Ed.* **2010**, *49*, 4042-4046.
42. Sugihara, S.; Blanazs, A.; Armes, S. P.; Ryan, A. J.; Lewis, A. L. *J. Am. Chem. Soc.* **2011**, *133*, 15707-15713.
43. Liu, G.; Qiu, Q.; Shen, W.; An, Z. *Macromolecules* **2011**, *44*, 5237-5245.
44. Chambon, P.; Blanazs, A.; Battaglia, G.; Armes, S. P. *Macromolecules* **2012**, *45*, 5081-5090.
45. Ladmiral, V.; Semsarilar, M.; Canton, I.; Armes, S. P. *J. Am. Chem. Soc.* **2013**, *135*, 13574-13581.
46. Figg, C. A.; Simula, A.; Gebre, K. A.; Tucker, B. S.; Haddleton, D.; Sumerlin, B. S. *Chemical Science* **2015**, *6*, 1230-1236.
47. Wan, W.-M.; Hong, C.-Y.; Pan, C.-Y. *Chem. Commun.* **2009**, 5883-5885.
48. Semsarilar, M.; Jones, E. R.; Blanazs, A.; Armes, S. P. *Adv. Mater.* **2012**, *24*, 3378-3382.
49. Zehm, D.; Ratcliffe, L. P. D.; Armes, S. P. *Macromolecules* **2012**, *46*, 128-139.
50. Karagoz, B.; Boyer, C.; Davis, T. P. *Macromol. Rapid Commun.* **2013**, *35*, 417-421.
51. Pei, Y.; Dharsana, N. C.; van Hensbergen, J. A.; Burford, R. P.; Roth, P. J.; Lowe, A. B. *Soft Matter* **2014**, *10*, 5787-5796.
52. Zhang, W.-J.; Hong, C.-Y.; Pan, C.-Y. *Macromolecules* **2014**, *47*, 1664-1671.
53. Bleach, R.; Karagoz, B.; Prakash, S. M.; Davis, T. P.; Boyer, C. *ACS Macro Lett.* **2014**, *3*, 591-596.
54. Semsarilar, M.; Ladmiral, V.; Blanazs, A.; Armes, S. P. *Polym. Chem.* **2014**, *5*, 3466-3475.
55. Gonzato, C.; Semsarilar, M.; Jones, E. R.; Li, F.; Krooshof, G. J. P.; Wyman, P.; Mykhaylyk, O. O.; Tuinier, R.; Armes, S. P. *J. Am. Chem. Soc.* **2014**, *136*, 11100-11106.
56. Houillot, L.; Bui, C.; Farcet, C. l.; Moire, C.; Raust, J.-A.; Pasch, H.; Save, M.; Charleux, B. *ACS Appl. Mater. Interfaces* **2010**, *2*, 434-442.
57. Deng, Y.; Yang, C.; Yuan, C.; Xu, Y.; Bernard, J.; Dai, L.; Gérard, J.-F. *J. Polym. Sci. A Polym. Chem.* **2013**, *51*, 4558-4564.
58. Fielding, L. A.; Derry, M. J.; Ladmiral, V.; Rosselgong, J.; Rodrigues, A. M.; Ratcliffe, L. P. D.; Sugihara, S.; Armes, S. P. *Chem. Sci.* **2013**, *4*, 2081-2087.
59. Dan, M.; Huo, F.; Zhang, X.; Wang, X.; Zhang, W. *J. Polym. Sci. A Polym. Chem.* **2013**, *51*, 1573-1584.
60. Tan, J.; Rao, X.; Yang, J.; Zeng, Z. *Macromolecules* **2013**, *46*, 8441-8448.
61. Shi, P.; Li, Q.; He, X.; Li, S.; Sun, P.; Zhang, W. *Macromolecules* **2014**, *47*, 7442-7452.
62. Huang, C.-Q.; Pan, C.-Y. *Polymer* **2010**, *51*, 5115-5121.
63. Warren, N. J.; Mykhaylyk, O. O.; Mahmood, D.; Ryan, A. J.; Armes, S. P. *J. Am. Chem. Soc.* **2014**, *136*, 1023-1033.
64. Zhao, W.; Gody, G.; Dong, S.; Zetterlund, P. B.; Perrier, S. *Polym. Chem.* **2014**, *5*, 6990-7003.
65. Sugihara, S.; Armes, S. P.; Blanazs, A.; Lewis, A. L. *Soft Matter* **2011**, *7*, 10787-10793.
66. He, W.-D.; Sun, X.-L.; Wan, W.-M.; Pan, C.-Y. *Macromolecules* **2011**, *44*, 3358-3365.
67. Semsarilar, M.; Ladmiral, V.; Blanazs, A.; Armes, S. P. *Langmuir* **2011**, *28*, 914-922.
68. Semsarilar, M.; Ladmiral, V.; Blanazs, A.; Armes, S. P. *Langmuir* **2013**, *29*, 7416-7424.

69. Rieger, J.; Stoffelbach, F.; Bui, C.; Alaimo, D.; Jérôme, C.; Charleux, B. *Macromolecules* **2008**, *41*, 4065-4068.
70. Zhang, W.; D'Agosto, F.; Boyron, O.; Rieger, J.; Charleux, B. *Macromolecules* **2012**, *45*, 4075-4084.
71. Rieger, J.; Zhang, W.; Stoffelbach, F.; Charleux, B. *Macromolecules* **2012**, *43*, 6302-6310.
72. Zhang, W.; D'Agosto, F.; Dugas, P.-Y.; Rieger, J.; Charleux, B. *Polymer* **2013**, *54*, 2011-2019.
73. Ratcliffe, L. P. D.; Blanazs, A.; Williams, C. N.; Brown, S. L.; Armes, S. P. *Polym. Chem.* **2014**, *5*, 3643-3655.
74. Binauld, S.; Delafresnaye, L.; Charleux, B.; D'Agosto, F.; Lansalot, M. *Macromolecules* **2014**, *47*, 3461-3472.
75. Zhang, X.; Boisson, F.; Colombani, O.; Chassenieux, C.; Charleux, B. *Macromolecules* **2014**, *47*, 51-60.
76. Carlsson, L.; Fall, A.; Chaduc, I.; Wagberg, L.; Charleux, B.; Malmstrom, E.; D'Agosto, F.; Lansalot, M.; Carlmark, A. *Polym. Chem.* **2014**, *5*, 6076-6086.
77. Zhang, X.; Cardozo , A. F.; Chen , S.; Zhang, W.; Julcour , C.; Lansalot, M.; Blanco , J.-F.; Gayet , F.; Delmas , H.; Charleux , B.; Manoury , E.; D'Agosto, F.; Poli , R. *Chem. Eur. J.* **2014**, *20*, 15505-15517.
78. Ihli, J.; Bots, P.; Kulak, A.; Benning, L. G.; Meldrum, F. C. *Adv. Funct. Mater.* **2013**, *23*, 1965-1973.
79. Jones, E. R.; Semsarilar, M.; Blanazs, A.; Armes, S. P. *Macromolecules* **2012**, *45*, 5091-5098.
80. Blanazs, A.; Madsen, J.; Battaglia, G.; Ryan, A. J.; Armes, S. P. *J. Am. Chem. Soc.* **2011**, *133*, 16581-16587.
81. Odian, G. *Principles of Polymerization, Fourth Edition*; Wiley, 2004.
82. Warren, N. J.; Mykhaylyk, O. O.; Ryan, A. J.; Williams, M.; Doussineau, T.; Dugourd, P.; Antoine, R.; Portale, G.; Armes, S. P. *J. Am. Chem. Soc.* **2015**, *137*, 1929-1937.
83. Atkins, P.; De Paula, J. *Physical Chemistry*; Oxford University Press, 2006.
84. Semsarilar, M.; Jones, E. R.; Armes, S. P. *Polym. Chem.* **2014**, *5*, 195-203.
85. Blanazs, A.; Armes, S. P.; Ryan, A. J. *Macromol. Rapid Commun.* **2009**, *30*, 267-277.
86. Lowenstam, H. A.; Weiner, S. *On Biomineralization*; Oxford University Press: New York, 1989.
87. Meldrum, F. C.; Cölfen, H. *Chem. Rev.* **2008**, *108*, 4332-4432.
88. Berman, A.; Hanson, J.; Leiserowitz, L.; Koetzle, T. F.; Weiner, S.; Addadi, L. *Science* **1993**, *259*, 776-779.
89. Kulak, A. N.; Iddon, P.; Li, Y.; Armes, S. P.; Cölfen, H.; Paris, O.; Wilson, R. M.; Meldrum, F. C. *J. Am. Chem. Soc.* **2007**, *129*, 3729-3736.
90. Kim, Y.-Y.; Ganesan, K.; Yang, P.; Kulak, A. N.; Borukhin, S.; Pechook, S.; Ribeiro, L.; Kröger, R.; Eichhorn, S. J.; Armes, S. P.; Pokroy, B.; Meldrum, F. C. *Nature Mater.* **2011**, *10*, 890-896.
91. Kulak, A. N.; Yang, P.; Kim, Y.-Y.; Armes, S. P.; Meldrum, F. C. *Chem. Commun.* **2014**, *50*, 67-69.
92. Kulak, A. N.; Semsarilar, M.; Kim, Y.-Y.; Ihli, J.; Fielding, L. A.; Cespedes, O.; Armes, S. P.; Meldrum, F. C. *Chem. Sci.* **2014**, *5*, 738-743.
93. Borukhin, S.; Bloch, L.; Radlauer, T.; Hill, A. H.; Fitch, A. N.; Pokroy, B. *Adv. Funct. Mater.* **2012**, *22*, 4216-4224.

94. Kim, Y.-Y.; Ribeiro, L.; Maillot, F.; Ward, O.; Eichhorn, S. J.; Meldrum, F. C. *Adv. Mater.* **2010**, *22*, 2082-2086.
95. Tomson, M. B. *J. Cryst. Growth* **1983**, *62*, 106-112.
96. Ketrane, R.; Saidani, B.; Gil, O.; Leleyter, L.; Baraud, F. *Desalination* **2009**, *249*, 1397-1404.